J Mater Sci (2010) 45:6200–6205
DOI 10.1007/s10853-010-4713-z

The effects of synthesis procedures on the structure and morphology of multiwalled carbon nanotubes (MWNTs)/titania (TiO_2) nanocomposites prepared by hydrothermal method

Huifang Xu · Jing Wang · Haijiao Zhang · Yudong Huang

Received: 25 January 2010 / Accepted: 11 June 2010 / Published online: 22 June 2010

Abstract The nanocomposites of multiwalled carbon nanotubes (MWNTs)/titania (TiO_2) were prepared by direct growth of TiO_2 nanocrystals onto carboxyl-modified MWNTs under hydrothermal condition. The structure and morphology of TiO_2 nanocrystals growing on MWNTs were tuned by adjusting acidity, reaction temperature, and reactant ratio. The results showed that a uniform layer of anatase TiO_2 nanocrystals on MWNTs could be achieved at proper synthesis parameters. Flowerlike assemblage of rutile TiO_2 nanocrystals was dispersed on MWNTs. The formation mechanism of MWNTs/TiO_2 nanocomposites was further provided.

Introduction

Since the discovery of carbon nanotubes (CNTs) in 1991 [1], CNTs have aroused intense interests because of their unique physicochemical properties. CNTs could be used in the fields of nano-devices, and biomaterial devices, etc. [2–6].

Carbon nanotubes, with long aspect ratio, are ideal one-dimensional nanomaterials, and suitable for being used as carrier to load functional nanoparticles. The improvement of modification methods on CNTs greatly propels their application in nanocomposites. Recently, a series of functional nanocomposites were prepared for application in the areas of catalysis, lithium ion batteries, gas detection, and supercapacitors [7–15]. Especially, CNTs/TiO_2 nanocomposites have attracted much attention recently because they combine the favorable properties of both CNTs and TiO_2 nanocrystals [16–24].

TiO_2 nanocrystals have been regarded as one of the most attractive semiconductor materials due to their high chemical stability, high dielectric constants, photocatalysis activity, and non-toxic property [25–27]. Up to now, the reports on CNTs/TiO_2 composites were focused on the method to immobilize TiO_2 nanocrystals on CNTs, and their application in the field of photocatalysis, etc. [16–24]. It was shown that anchoring TiO_2 nanocrystals on CNTs is an efficient approach to enhance the photocatalytic activity because CNTs present high surface areas, high electron conductions, and high adsorption capacities [16–19]. The biocompatible property of CNTs could be improved by constructing CNTs/TiO_2 nanocomposites, and the electrodes modified with the nanocomposites are promising in the bioanalytical applications [24]. The key problem for the exploration of CNTs/nanoparticle composites as functional materials is the ability in controllable anchor of nanoparticles on the surface of CNTs with combination of the control on physicochemical properties of nanoparticles. The properties of TiO_2 are greatly dependent on crystalline phase, particle size, and morphology, which could be controlled by adjusting the preparation conditions [28]. With the increased interests on CNTs/TiO_2 nanocomposites, there is a need to investigate the growth process of TiO_2 nanocrystals onto multiwalled carbon nanotubes (MWNTs) for controlling over their structure and morphology.

In this article, the growth of TiO_2 nanocrystals on modified MWNTs by hydrothermal process was investigated. The study indicated that coating a continuous

H. Xu (✉) · J. Wang · Y. Huang
School of Chemical Engineering and Technology, Harbin Institute of Technology, Harbin 150001, China
e-mail: xuhf@hit.edu.cn

H. Zhang
School of Materials Science and Engineering, Harbin Institute of Technology, Harbin 150001, China

layer of TiO_2 nanoparticles could be achieved by good dispersion of MWNTs in TiO_2 precursor sols in prior. The loading amount, crystalline phase, morphology of TiO_2 nanocrystals growing on MWNTs were adjusted by tuning the reaction factors. The structure and morphology of the nanocomposites were investigated by scanning electron microscopy (SEM), X-ray powder diffraction (XRD), Fourier transform infrared spectra (FTIR), thermogravimetric analysis (TGA), and differential thermal analysis (DTA).

Experimental section

Syntheses

Raw materials

Commercially available pristine MWNTs (CVD method, 95%) used here were purchased from Shenzhen Nanotech Port Co., Ltd, China. All following materials were used as received: tetrabutyl titanate (TBT, 98%), nitric acid (HNO_3, 68%), and absolute ethanol.

Carboxylic functionalization of MWNTs

Multiwalled carbon nanotubes were functionalized by refluxing in HNO_3 for 20 h, washed with deionized water, and separated by percolation until the pH value of filtrate was about 6.

Preparation of MWNTs/TiO_2 nanocomposites

TiO_2 sol was first prepared. Nitric acid was used to adjust the acidity of TiO_2 sols. A typical procedure was as follows: TBT (0.08 mL), ethanol (2.0 mL), and 2 M (mol/L) nitric acid (2.5 mL) were mixed under stirring at room temperature for 1 h to form a concentrated transparent sol. By adding mixture of ethanol and distilled water to above sol until a total volume of 25 mL, the final sol was obtained for use. 25 mg acid-treated MWNTs was added to the above sol (25 mL) under sonication and further stirred for 2 h so that the sol was thoroughly mixed with MWNTs. The mixture of MWNTs with sol was transferred into an autoclave and heated at 120 or 180 °C for 24 h to form MWNTs/TiO_2 composites. The resulting powders were washed by ethanol and deionized water, and finally, collected by freezing drying.

Characterization

Scanning electron microscopy measurement was performed with a HITACHI S-4300 instrument operated at an accelerating voltage of 15 kV. The samples were dried at ambient temperature and vacuum sputtered with Pt about an average size of 3 nm. Wide-angle XRD (Rigaku D/max-2500) was used to characterize the crystalline phase. The thermal properties of the nanocomposites were determined by TGA and DTA with Netzsch STA 449 C instrument in the temperature range of 30–800 °C in flowing air at a heating rate 10 °C/min. FTIR were recorded using a Bruker Equinox 55 spectrometer with samples pressed into KBr pellets.

Results and discussion

Structure characterization of MWNTs and MWNTs/TiO_2

MWNTs were first treated by acid prior to use. The pristine MWNTs tend to aggregate into bundles due to the Van der Waals force among MWNTs [29]. Compared with pristine MWNTs, acid-treated MWNTs could be stably dispersed in distilled water for several weeks, but the stability of acid-treated MWNTs in initial TiO_2 sol was dependent on acidity. The stable dispersion of MWNTs in starting TiO_2 precursor sol was obtained when the amount of acid (2 M) was lower than 2.5 mL. The higher acidity will lead to the aggregation of acid-treated MWNTs in starting TiO_2 sol.

The morphology of acid-treated MWNTs is observed from a typical SEM image in Fig. 1a. The average outer diameter is about 40–60 nm. The surface morphology is smooth. MWNTs/TiO_2 composites were prepared according to reaction parameters specified in Table 1. Figure 1b, c shows the SEM images of the typical MWNTs/TiO_2 nanocomposite (sample2). Compared with acid-treated MWNTs, the surface morphology of nanocomposites became rougher. In the enlarged SEM image (Fig. 1c), it is shown that spherical nanoparticles about 15 nm in diameter are compactly coated on acid-treated MWNTs. Figure 2 presents the XRD results of the nanocomposites. The peaks at 2θ ca. 26.2° and 43.4° are characteristic of CNTs [30]. The spherical nanoparticles on MWNTs formed in low acidity (sample1 and sample2) are indexed as anatase phase by XRD results (curve a and curve b in Fig. 2), on the basis of Joint Commission on Powder Diffraction Standards data (JCPDS No. 21-1272). The low acidity for sample1 results in the formation of fine anatase crystals and thus the wider XRD diffraction peaks [28], shown in curve a in Fig. 2. The diffraction peaks of sample2 become narrower and stronger than those of sample1, shown in curve b in Fig. 2, implying that enhancing acidity facilitates further growth of the nanocrystals. The anatase TiO_2 peak (101) at reflection plane 2θ 25.3° overlaps with peak of MWNTs at 2θ 26.2°.

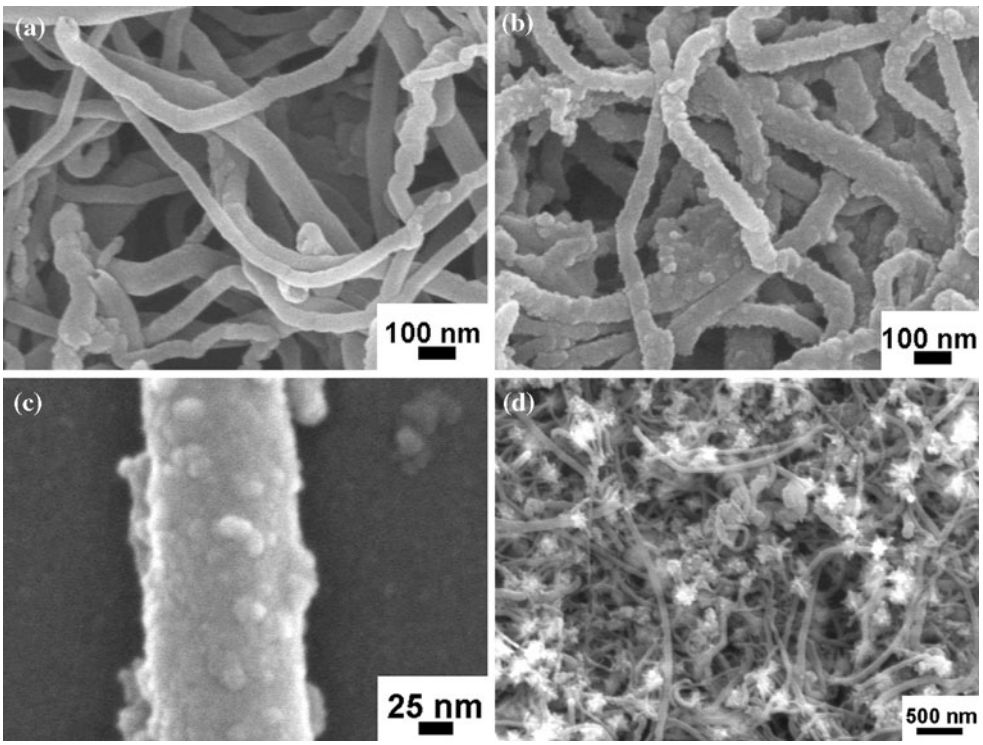

Fig. 1 SEM images. **a** Acid-treated MWNTs, **b** sample2, **c** an enlarged SEM image of a typical composite nanotube of sample2, **d** sample3

Table 1 Synthesis parameters

Sample	MWNTs (mg)	TBT (mL)	$[H^+]$ (M)/V (mL)	EtOH (mL)	V_{total} (mL)	Temperature (°C)
1	25	0.08	2/0.4	4.0	25	120
2	25	0.08	2/2.5	4.0	25	120
3	25	0.08	2/5	4.0	25	120
4	25	0.08	2/0.4	4.0	25	180
5	25	0.30	2/18.75	4.0	25	180

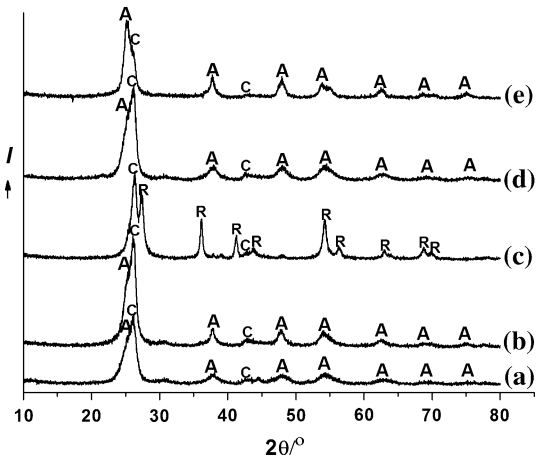

Fig. 2 XRD patterns of MWNTs/TiO_2 composites. *a* Sample1, *b* sample2, *c* sample3, *d* smaple4, *e* sample5. The letters *A*, *R*, and *C* stand for anatase TiO_2 (JCPDS No. 21-1272), rutile TiO_2 (JCPDS No. 21-1276), and MWNTs, respectively

When acidity of TiO_2 precursor sol was increased to 5 mL/2 M, acid-treated MWNTs could not be stably dispersed in the starting TiO_2 sol. After hydrothermal reaction, as a result, flowerlike assemblage is grown on MWNTs as being shown in Fig. 1d. XRD pattern (curve c in Fig. 2) indicates that the composite is composed of rutile TiO_2 (JCPDS No. 21-1276) and CNTs. The formation of TiO_2 on MWNTs is further investigated by varying other reaction parameters (sample4 and sample5). With increasing reaction temperature, the crystallization of anatase is enhanced, compared curve a with curve d in Fig. 2. Although the acidity of TiO_2 sol was high for sample5, increasing in reaction temperature and feeding amount of TBT led to forming MWNT/anatase TiO_2 composites, which is certified in curve e of Fig. 2.

FTIR spectra were conducted to investigate the functional groups of samples. Curves a and b in Fig. 3 show the FTIR results of pristine MWNTs and acid-treated MWNTs,

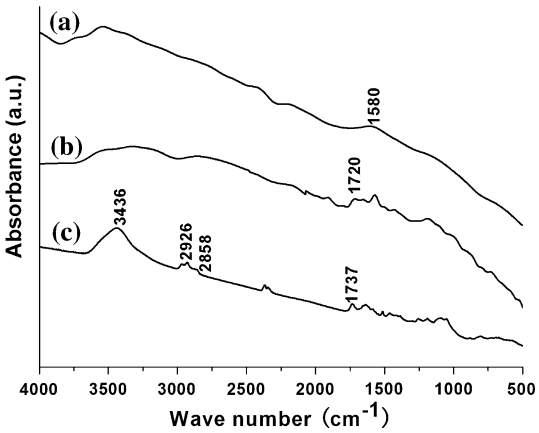

Fig. 3 FTIR results of the typical samples. *a* MWNTs, *b* acid-treated MWNTs, *c* sample2

respectively. The characteristic band in 3400 cm^{-1} becomes stronger in the latter than in the former, implying the concentration of hydroxyl is increased after acid treatment. The carboxyl groups of acid-treated MWNTs are confirmed by FTIR with stretching band at 1720 cm^{-1} as shown in curve b of Fig. 3. The adsorption peak of carboxyl groups of typical MWNTs/TiO_2 composite shown in curve c is moved to 1737 cm^{-1}, indicating the formation of covalent linkage of TiO_2 with acid-treated MWNTs [31].

Thermal properties by TGA–DTA

Thermal properties of typical samples are investigated by TGA and DTA analyses. Figure 4a shows that MWNTs could be entirely degraded under flowing air. Therefore, the residual mass by TGA is the content of TiO_2 in MWNTs/TiO_2 composites. By adjusting ratio of TBT to MWNTs, the amount of TiO_2 is changed from 34.0 wt% (sample2) to 58.3 wt% (sample5) according to TGA analyses. DTA curve for acid-treated MWNTs shows two peaks at 533 and 626 °C, due to the thermal oxidative degradation of MWNTs. Two peaks at about 260 and 600 °C are shown in DTA curves of MWNTs/TiO_2 composites. The first exothermal reaction corresponds to the removal of small molecules from TBT. The second one is attributed to degradation of MWNTs. The degradation temperature of MWNTs is in the range of 500 to 700 °C. T_{MAX} (maximum degradation temperature of MWNTs from DTA) of MWNTs/TiO_2 composites are changed according to different reaction conditions. T_{MAX} shows a maximum for sample3, in which MWNTs/rutile TiO_2 composite was formed (Table 2).

Formation mechanism analyses

The formation of TiO_2 with different crystalline phases and morphologies on carboxyl-functionalized MWNTs is analyzed according to the results. The low pH value is a decisive factor for forming TiO_2 crystallites by liquid methods because proton ions can expedite hydrolysis and slow down the condensation in the acid-catalyzed sol–gel process [32]. In comparison, the conventional sol–gel process usually involves uncontrollable hydrolysis and condensation, and thereby results in the formation of disordered structure. Herein, the crystallization of TiO_2 was conducted under acidic solution. The formation mechanism for crystalline phase of TiO_2 on MWNTs is consistent with that of bulk TiO_2 nanocrystals. TiO_2 nanocrystals can grow from TiO_6 octahedra. From above results, we can presume that amorphous TiO_2 sol was produced at the initial reaction stage. The amorphous sol composed of aggregate TiO_6 octahedra will be dispersed into discrete TiO_6 octahedra by protonation of the surface Ti–OH groups giving Ti–OH_2^+ under acidic solution. Ti–O–Ti oxygen bridge bonds are generated by combining the protonated surfaces with –OH groups of other TiO_6 octahedra and then eliminating a water molecule. The phase formation depends on linkage manners between TiO_6 octahedra [33–37]. The protonation process followed by the face-sharing from the TiO_6 octahedra will be beneficial for formation of anatase phase. This process could be promoted by increasing reaction temperature, which showed the crystallization was enhanced at high temperature [28]. Further, decrease of the reaction rate is expected to favor formation of rutile TiO_2. In the case of sample3, when compared with sample1, sample2, and sample4, the lower reaction temperature and higher acidity of the sol slow down the reaction rate, which results in the preferred formation of rutile TiO_2 nanocrystals [34, 38]. Gopal et al. considered this problem from the aspect of thermodynamic stability that the activation energies for forming rutile, anatase, amorphous TiO_2 should be described as $Q_{rutile} < Q_{anatase} < Q_{amorphous}$ [34]. Therefore, it is proposed that rutile phase could be obtained at the lowest reaction rate; at the fastest reaction rate, amorphous phase will be produced; anatase phase will be obtained when the reaction rate is between the above two. In the present study, rutile TiO_2 were formed in sample3, in which low reactant concentration and high acidity facilitated the olation reaction proceeding in the equatorial plane, and finally forming a linear chain polymer, which is only structurally compatible with rutile [33]. Additionally, the excessive increase in TBT concentration and temperature will accelerate the reaction, which promotes the formation of mesostable anatase TiO_2, although the acidity of sample5 is high.

On the other hand, the dispersion of acid-treated MWNTs in starting TiO_2 sol was found to depend on its acidity, leading to different morphology of MWNTs/TiO_2 composites at varied acidity. The formation process under different acidity was illustrated in Fig. 5. The acid-treated MWNTs are functionalized by carboxyl groups on surface.

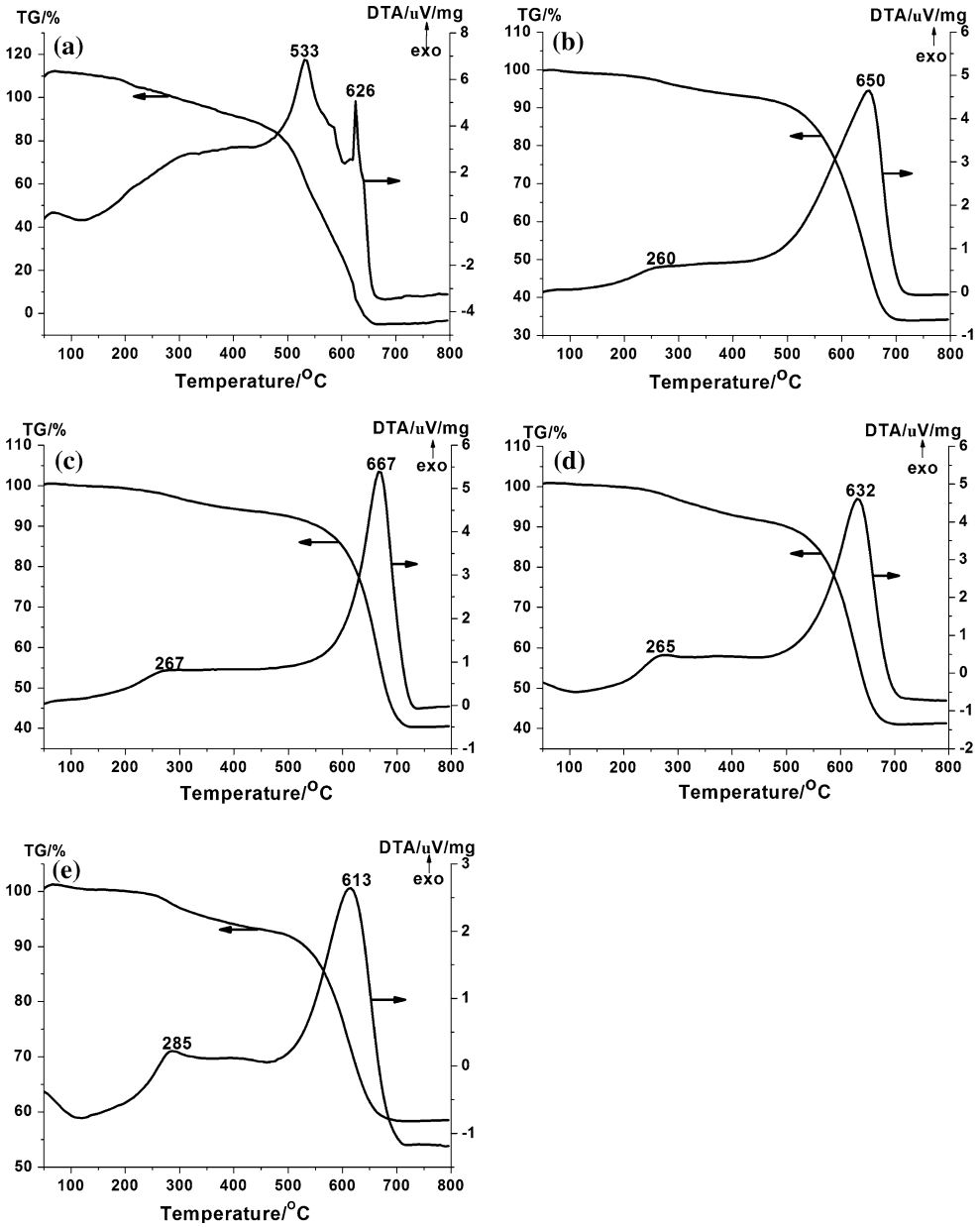

Fig. 4 TGA and DTA results. **a** Acid-treated MWNTs, **b** sample2, **c** sample3, **d** sample4, **e** sample5

Table 2 Thermal parameters characterized by TGA and DTA

No.	MWNTs	Sample2	Sample3	Sample4	Sample5
Residual (%)	0	34.0	40.4	41.1	58.3
Oxidation peaks	533/626	260/650	267/667	265/632	285/613

The deprotonation of carboxyl groups will give negatively charged MWNTs, when pH values of TiO_2 sol are above that of deprotonation point of carboxyl groups. The adsorption between negatively charged MWNTs with positively charged Ti-OH_2^+ promotes the dispersion of MWNTs in TiO_2 sol. An intact coat of anatase TiO_2 on MWNTs could be achieved at relatively low acidity. Comparably, the protonation of carboxyl groups on acid-treated MWNTs results in reduction of their stability in high acidic TiO_2 sol and weak interaction of TiO_2 with MWNTs. The nucleation sites on MWNTs decreased when high acidic sols were applied, therefore resulting in assemblage of rutile TiO_2 on surface of MWNTs. Additionally, with high acidity but increasing both reaction temperature and TBT content, the fast linkage of TiO_6 octahedra resulted in forming anatase phase on MWNTs.

Conclusions

In this article, MWNTs/TiO_2 nanocomposites were prepared by hydrothermal growth of TiO_2 nanocrystals on

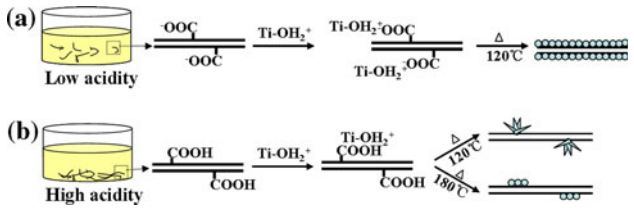

Fig. 5 A schematic drawing illustrates formation process of MWNTs/TiO_2 with different reaction parameters. **a** Uniform layer of anatase nanocrystals on MWNTs formed at low acidity and 120 °C, **b** flowerlike assemblage of rutile TiO_2 nanocrystals on MWNTs formed at high acidity and 120 °C, and assemblage of anatase TiO_2 nanocrystals on MWNTs formed at high acidity and 180 °C

functionalized MWNTs. The morphology and crystal phase were tuned by adjusting reaction parameters. The acidity of starting TiO_2 sol played an important role in tailoring TiO_2 phases and morphologies of composites. The intact coat of anatase titania was achieved by well dispersing MWNTs in TiO_2 sol and further growth. The flowerlike assemblage of rutile TiO_2 on MWNTs was obtained due to the weak dispersion of acid-treated MWNTs in strong acidic TiO_2 sol.

Acknowledgement This project was supported by Natural Scientific Research Innovation Foundation in Harbin Institute of Technology (HIT. NSRIF. 2009124) and the postdoctoral research foundation in Harbin Institute of Technology.

References

1. Iijima S (1991) Nature 354:56
2. Yi H, Song H, Chen X (2007) Langmuir 23:3199
3. Polizu S, Savadogo O, Poulin P, Yahia L (2006) J Nanosci Nanotechnol 6:1883
4. Sano M, Kamino A, Okamura J, Shinkai S (2002) Nano Lett 2:531
5. Lee GW, Lee JI, Lee SS, Park M, Kim JY (2005) J Mater Sci 40:1259. doi:10.1007/s10853-005-6947-8
6. Shi J, Wang Z, Li HL (2007) J Mater Sci 42:539. doi:10.1007/s10853-006-1043-2
7. Ma C, Zhang W, Zhu Y, Ji L, Zhang R, Koratkar N, Liang J (2008) Carbon 46:706
8. Li X, Liu Y, Fu L, Cao L, Wei D, Wang Y (2006) Adv Funct Mater 16:2431
9. He D, Yang L, Kuang S, Cai Q (2007) Electrochem Commun 9:2467
10. Shin HS, Jang YS, Lee Y, Jung Y, Kim SB, Choi HC (2007) Adv Mater 19:2873
11. Zhu Y, Elim HI, Foo YL, Yu T, Liu Y, Ji W, Lee JY, Shen Z, Wee ATS, Thong JTL, Sow CH (2006) Adv Mater 18:587
12. Zhao C, Ji L, Liu H, Hu G, Zhang S, Yang M, Yang Z (2004) J Solid State Chem 177:4394
13. Yang YK, Qiu SQ, Cui W, Zhao Q, Cheng XJ, Li RKY, Xie XL, Mai YW (2009) J Mater Sci 44:4539. doi:10.1007/s10853-009-3687-1
14. Deng MG, Yang BC, Zhang ZA, Hu YD (2005) J Mater Sci 40:1017. doi:10.1007/s10853-005-6523-2
15. Chang QF, Zhao K, Chen X, Li MQ, Liu JH (2008) J Mater Sci 43:5861. doi:10.1007/s10853-008-2827-3
16. Wang S, Ji L, Wu B, Gong Q, Zhu Y, Liang J (2008) Appl Surf Sci 255:3263
17. Yao Y, Li G, Ciston S, Lueptow RM, Gray KA (2008) Environ Sci Technol 42:4952
18. Akhavan O, Abdolahad M, Abdi Y, Mohajerzadeh S (2009) Carbon 47:3280
19. An G, Ma W, Sun Z, Liu Z, Han B, Miao S, Miao Z, Ding K (2007) Carbon 45:1795
20. Huang Q, Gao L (2003) J Mater Chem 13:1517
21. Ji L, Wang Z, Li Z, Liang J (2008) Mater Lett 62:1979
22. Li J, Tang S, Lu L, Zeng HC (2007) J Am Chem Soc 129:9401
23. Li X, Niu J, Zhang J, Li H, Liu Z (2003) J Phys Chem B 107:2453
24. Shen Q, You SK, Park SG, Jiang H, Guo DD, Chen BA, Wang XM (2008) Electroanalysis 20:2526
25. Zubavichus YV, Slovokhotov YL, Nazeeruddin MK, Zakeeruddin SM, Gratzel M, Shklover V (2002) Chem Mater 14:3556
26. Wu J, Zhang T, Zeng Y, Hayakawa S, Tsuru K, Osaka A (2005) Langmuir 21:6995
27. Yu XX, Yu JG, Cheng B, Jaroniec M (2009) J Phys Chem C 113:17527
28. Yu JG, Yu HG, Cheng B, Zhao XJ, Yu JC, Ho WK (2003) J Phys Chem B 107:13871
29. Yang Y, Xie X, Wu J, Mai Y (2006) J Polym Sci A Polym Chem 44:3869
30. Lee SW, Sigmund WM (2003) Chem Commun 6:780
31. Wang Q, Yang D, Chen D, Wang Y, Jiang Z (2007) J Nanopart Res 9:1087
32. Xu HF, Wei W, Zhang CL, Ding SJ, Qu XZ, Liu JG, Lu YF, Yang ZZ (2007) Chem Asian J 2:828
33. Guo W-L, Wang X-K (2004) J Mater Sci 39:3265. doi:10.1023/B:JMSC.0000025875.71970.17
34. Gopal M, Moberly Chan WJ, Jonghe LC (1997) J Mater Sci 32:6001. doi:10.1023/A:1018671212890
35. Ayouchi R, Martín F, Ramos-Barrado JR, Leinen D (2000) Surf Interface Anal 30:565
36. Scolan E, Sanchez C (1998) Chem Mater 10:3217
37. Yin H, Wada Y, Kitamura T, Kambe S, Murasawa S, Mori H, Sakata T, Yanagida S (2001) J Mater Chem 11:1694
38. Li Y, Lee N, Hwang DS, Song JS, Lee EG, Kim SJ (2004) Langmuir 20:10838